Assessing of Urban Vegetation Biomass in Combination with LiDAR and High-resolution Remote Sensing Images

Ya Zhang & Zhenfeng Shao

Published online: 02 Dec 2020.

Submit your article to this journal ⬈

View related articles ⬈

View Crossmark data ⬈

Taylor & Francis
Taylor & Francis Group

Check for updates

Assessing of Urban Vegetation Biomass in Combination with LiDAR and High-resolution Remote Sensing Images

Ya Zhang and Zhenfeng Shao

State Key Laboratory of Information Engineering in Surveying, Mapping and Remote Sensing, Wuhan University, Wuhan, China

ABSTRACT

The urban vegetation ecosystem is a vegetation ecosystem that is deeply influenced by human beings. The rapid urbanization process brings a great influence on the growth environment of urban vegetation. Urban vegetation has a certain mitigating effect on the urbanization process. It is irreplaceable by other urban ecosystems in functions such as maintaining atmospheric carbon–oxygen balance, reducing heat island effects, purifying, and beautifying the urban environment. At present, the estimation of aboveground biomass (AGB) mainly focuses on the original forest, grassland, desertification vegetation and crops, and the data sources are mostly medium- and low-resolution data such as Land Remote-Sensing Satellite Thematic Map (Landsat TM), Enhanced Thematic Mapper Plus (ETM+), and Moderate Resolution Imaging Spectroradiometer (MODIS). Compared with the research objects such as forest and grassland, urban vegetation has higher heterogeneity of underlying surface within the city scope, and there are more mixed pixels of medium- and low-resolution data. Therefore, high-resolution data are needed for classification and estimation. This study uses Light Detection and Ranging (LiDAR) data to expand the sample size, combines high-resolution image data to classify urban vegetation areas, and quantitatively estimates and inverts biomass. The spatial and temporal variation of urban vegetation biomass was analysed by comparing the inversion accuracy of five different models and the advantages and disadvantages of the research models. The research results show that: (1) In the absence of urban forest sample points, the biomass background data are expanded with the help of LiDAR data and more data is provided for further inversion; (2) Through five model method comparison experiments, the optimal method for estimation is based on the Random Forest (RF) model; (3) Analysed the changes of urban vegetation in the study area in the past 10 years, the development of different types of urban vegetation has experienced a trend of increasing first and then decreasing. Due to the high heterogeneity of features in urban areas, this study improved the inversion accuracy of estimating urban vegetation biomass by classification, and provided reference value and the basis for urban ecological management and regional planning.

CONTACT Zhenfeng Shao ✉ shaozhenfeng@whu.edu.cn State Key Laboratory of Information Engineering in Surveying, Mapping and Remote Sensing, Wuhan University, Wuhan, China

1. Introduction

Climate warming and the role of forest biomass in forest sequestration and greenhouse gas emissions caused by deforestation have received considerable attention. The surface biomass accounts for about 30% of the total carbon pool of terrestrial ecosystems, and the quantitative estimation of vegetation biomass provides an important reference for global carbon reserves and carbon cycle studies (Liu et al. 2019). Therefore, accurate measurements of vegetation biomass and other biophysical parameters are crucial for a better understanding of the global carbon cycle and global warming. Estimating the biomass of urban vegetation on a regional scale is important for understanding vegetation growth, carbon assimilation process, and forest ecosystem (Mincey, Schmitt-Harsh, and Thurau 2013). In the construction of the urban ecological environment, vegetation plays an important role in purifying air and water body, weakening urban heat island effect (Shao Z et al. 2020b), suppressing noise, reducing wind speed, increasing surface runoff and regulating urban microclimate (Kumar and Mutanga 2017). Therefore, urban vegetation has a good indication of the urban ecological environment (Wilson et al. 2003). Accurate, rapid, and effective estimation and monitoring of urban vegetation biomass and its spatial distribution pattern can understand the basis of the carbon cycle and energy flow, and also the basis for measuring the role of urban vegetation in ecological regulation, environmental protection. It can provide a quantitative basis for the evaluation of the large-scale ecological quality and the effectiveness of forestry and ecological construction.

Remote-sensing data are widely used in various aboveground biomass (AGB) mapping, using spectral features obtained from satellite images to estimate parameters such as vegetation index, texture features, and Leaf Area Index (LAI) that is highly related to AGB (Fung and Siu 2000; Zhang et al. 2014). Over the years, AGB has been estimated using remote-sensing reflectance and various vegetation indices. Previous studies can be broadly divided into two categories. The first is the research status of natural ecosystem biomass estimation in forest and grassland. Zhang et al. (2014) combined the high-resolution LAI data and the maximum height of the canopy to evaluate the uncertainty of the California forest area through a remote-sensing parameter model, and accurately described the changes and trends of forest biomass. Zhang R et al (2019) used ground observation, Moderate Resolution Imaging Spectroradiometer (MODIS) data, climate and topography data and combined with historical ground survey data to produce a 1 km resolution estimation map of subtropical regional forest biomass, which not only improved the estimation accuracy of biomass but also emphasized the importance of the subtropical forest to regional biomass estimation. Jin et al. (2014) established a regression model of ground quadrate biomass and remote-sensing spectral data based on the measured data of xilingol league sample site in Inner Mongolia and five consecutive years of MODIS remote-sensing data, and analysed the spatial and temporal distribution characteristics of grassland grass yield by using the obtained optimal model. Muukkonen and Heiskanen (2005) constructed a forest biomass estimation model based on the spectral characteristics of the image by using neural network and regression. Li et al. (2013) estimated the grassland aboveground biomass of multi-temporal remote-sensing data based on a statistical model and artificial neural network method, and compared the estimation accuracy of the two methods. Most of the studies in this part focus on typical vegetation ecosystems in large areas.

Another type is the current status of urban vegetation monitoring research. Urban vegetation refers to trees as the main body in the city and its surrounding areas, and its surroundings, reaching a certain scale and coverage, which can have an important impact on the surrounding environment, and has obvious ecological and cultural values body. The monitoring of urban vegetation in foreign countries began in the 1970s, and many places use a combination of data to regularly monitor urban vegetation (Li X et al. 2019). However, the current monitoring of urban vegetation mainly focuses on the quantitative study of the spatial structure and distribution of urban vegetation using landscape ecological indicators, and few studies have conducted quantitative inversion studies from the aspect of vegetation biomass (Ren et al. 2017). Tao et al. (2013) explored the interaction between urban green space and residential land, and analysed the combination of quantitative research and planning of urban green space by using landscape pattern index method and network analysis method by analysing the spatial and temporal dynamic changes of urban vegetation and structure, and its application to the evaluation of ecosystem services are discussed. Wang et al. (2015) estimated the spatial distribution of forest leaf biomass in Shanghai city by combining regression analysis with spatial analysis based on the measured leaf biomass data of the sample site from June 2011 to June 2012 and the remote-sensing information of the same period, and discussed the remote-sensing estimation method of forest leaf biomass at the regional scale. Johnson (2013) and Zhou, Yu, and Qin (2014) used multi-source data and object-based change detection to extract and analyse vegetation changes at multiple levels. Although great progress has been made in using various remote-sensing data to improve the spatial explicit AGB estimation, there are still large uncertainties in the local scale of AGB regional estimation. Due to the different utilization modes of urban vegetation and the influence of geographical environment and other factors, most research areas have different conditions. In the actual study, appropriate image data and algorithms should be selected according to different monitoring scales to estimate biomass.

Fast and accurate image classification is the basis for the application of remote-sensing technology. With the continuous progress of remote-sensing technology, the number of bands ranges from single band to hyperspectral, and the resolution ranges from kilometres to metres (Gao et al. 2013; Mutanga, Adam, and Cho 2012). It also puts forward higher requirements for its classification and recognition technology (Ali et al. 2015). The results of object-oriented classification can be used to implement the quantitative analysis of dynamic change monitoring (Willhauck et al. 2000). Urban vegetation and environmental monitoring are quite different from grassland, forest, and other regional ecosystems. The city contains complex types of ground features, resulting in complex underlying surfaces and different vegetation planting structures (Shao et al. 2020d). Unlike grasslands or forests, there are relatively single underlying surface types and pure vegetation coverage areas. Different vegetation environments in urban landscapes may cause slight changes. The characteristics of vegetation landscapes in urban areas are highly heterogeneous (Rafiee, Mahiny, and Khorasani 2009). Many forest patches in the city play an important role in the urban vegetation ecosystem. At the same time, the urban vegetation also includes green vegetation such as grassland, so it is necessary to consider the classification of urban vegetation.

Aerial images have the characteristics of high spatial resolution and can reflect the canopy characteristics of ground vegetation. However, due to the shortcomings of spatial distribution and low spectral resolution of aerial images, large area monitoring cannot be realized. At the same time, the acquisition cost of aerial images is high, and it is easy to get

data due to weather conditions (Lucas, Lee, and Bunting 2008). Satellite remote-sensing image data due to its wide coverage, access to convenient, revisit cycle short, etc., in the research of urban vegetation coverage has been widely used (Wallis et al. 2019), but due to its resolution cannot be achieved to distinguish the vegetation canopy of a finer level, so in this study, consider using multi-source data to fill in the form of a single data source faults. In the urban vegetation ecosystem, the estimation of vegetation in the entire study area requires the use of multi-source satellite data to avoid the limitation of a single data source. Monitoring and analysis are performed to varying degrees according to areas where human activities are concentrated and some ecologically fragile areas (Guo Y et al. 2012).

In this study, we will classify the features in the study area, extract the vegetation area in the features, and divide the urban vegetation into forest and grassland for estimation (Clark 2020). Obtaining the 'truth value' of the biomass in the study area based on aerial Light Detection and Ranging (LiDAR) data can fully reflect the changes in the vegetation structure and growth status of the study area. Using 10 years of high-resolution optical images within the study area, parameterized and non-parameterized models are used to compare the performance of the selected biomass attribute prediction model method, construct the urban vegetation biomass inversion model and verify the accuracy of the results, so as to realize the inversion and monitoring of urban vegetation biomass. Main realizations: (1) examining the effectiveness of using LiDAR data to augment sample data, (2) establishing urban vegetation biomass estimation models by coupling measured data with WorldView data, (3) making a spatiotemporal map of urban vegetation attributes with a resolution of 2 m, and (4) exploration and dynamic analysis of urban vegetation spatial pattern in Hengqin research area, Zhuhai from 2009 to 2018. The model results are conducive to promoting the application of biomass estimates based on aerial LiDAR images to replace the measured data in the field, especially for areas where it is difficult to obtain sufficient and representative field survey data. Through the analysis of different vegetation conditions in the study area in time and space, it can provide a reference for urban development planning and construction of the ecological city.

2. Materials and methods

2.1. Study area

The study area is located at 113°31'42.78" E and 22°6'39.57" N (Figure 1). It is mainly composed of large and small Hengqin islands. Dahengqin mountain range is undulating, the mountain range is basically east-to-west direction, the highest altitude is 457.7 m. Xiaohengqin mountain slope is gentle, the highest altitude is about 130 m. The central ditch located in the central area is 7 km east to west and 2 km wide from north to south. The study area is located south of the tropic of cancer and belongs to the South Subtropical Monsoon Region. It has plenty of sunshine and abundant rainfall. The average annual temperature is 22°C to 23°C; the average seawater temperature is 22.4°C, the average annual precipitation is 2015.9 nm, and the annual water storage is 36.54 million m^3. It has three well-protected natural ecosystems of ocean, forest, and wetland. It is surrounded by waterbodies, with beautiful coastlines and lush vegetation. The coastline around the island is 50 km long. The environmental quality of study area New District is excellent, with an annual average PM2.5 concentration of 28 g m^{-3}.
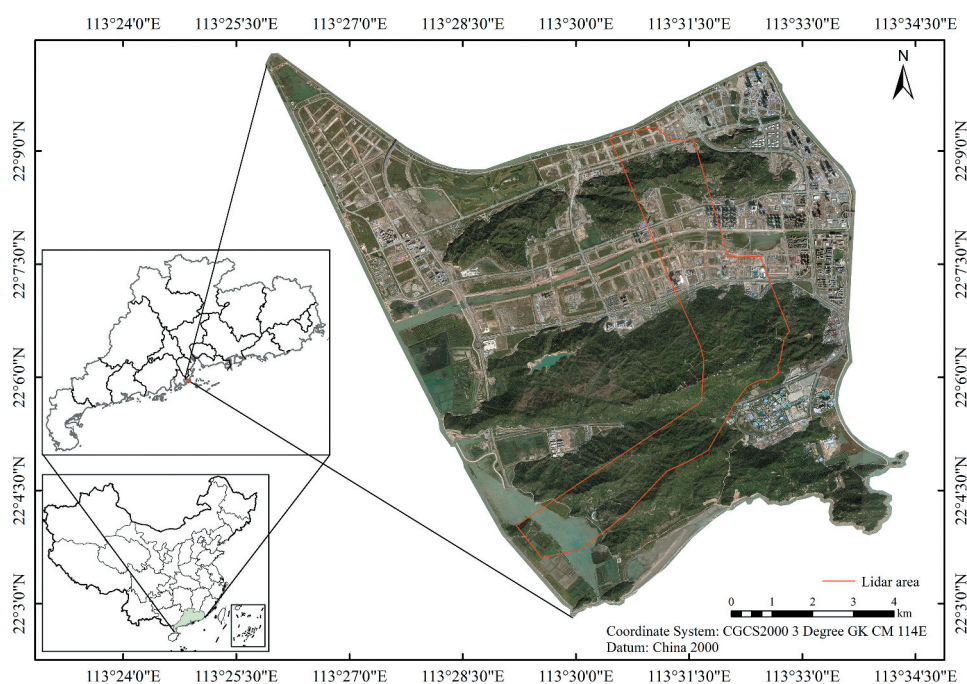
Figure 1. Sketch map of study area.

2.2. Data and pre-processing

This paper uses two types of remote-sensing high-resolution multispectral image data and LiDAR point cloud data, as well as ground-based sample data. Data sources, pre-processing, and factor extraction are described in detail in the following three sections of the summary.

2.2.1. Multispectral data

In the experiment, a total of 10 years of optical data from Worldview-2 (WV-2), Worldview-3 (WV-3), and GaoFen-2 (GF-2) are used for experimental analysis. The optical data used for the model inversion in this study is the 2018 WV-3 product. The spatial resolution of the multispectral band is 1.43 m, and the cloud cover is 0. The images are clear and can cover the entire research area to meet the experimental requirements. The spatial projection type of remote-sensing image data is UTM-WGS84. Radiation calibration and atmospheric correction were performed on the image in ENVI 5.4 software.

All images used in this study are summarized in Table 1. Details of each dataset are introduced in the following subsection.

2.2.2. LiDAR data

The drone is equipped with the SKYEYE SE-J500B airborne LiDAR system, and a study area of 20 km^2 is selected as the flight area. The data were collected from 28 July to 31 July. LiDAR strip point cloud data with an accuracy of 1: 1000 were obtained by drone. LiDAR point cloud data preprocessing is carried out in Terrasolid, which mainly includes singular

Table 1. Characteristic of multispectral data used in this study.

		Spectral band (nm)			
Year	Sensor	Blue	Green	Red	NIR
2018	Wordview-3	450 to 510	510 to 580	630 to 690	770 to 895
2017	Wordview-3	450 to 510	510 to 580	630 to 690	770 to 895
2016	GaoFen-2	450 to 520	520 to 590	630 to 690	770 to 890
2015	Wordview-2	450 to 510	510 to 580	630 to 690	770 to 895
2014	Wordview-2	450 to 510	510 to 580	630 to 690	770 to 895
2013	Wordview-2	450 to 510	510 to 580	630 to 690	770 to 895
2012	Wordview-2	450 to 510	510 to 580	630 to 690	770 to 895
2011	Wordview-2	450 to 510	510 to 580	630 to 690	770 to 895
2010	Wordview-2	450 to 510	510 to 580	630 to 690	770 to 895
2009	Wordview-2	450 to 510	510 to 580	630 to 690	770 to 895

value removal, ground and non-ground point classification, normalized height calculation, and orthorectification. After the optical image is used as a reference, the normalized height image is geometrically corrected. The terrain point normalized vegetation point is obtained by subtracting the ground point elevation from the vegetation point elevation, and is used to extract single tree or stand parameters, or generate Canopy Height Model (CHM) to extract related parameters (Shao, Zhang, and Wang 2017). LiDAR variables at the sample level were further extracted, which included canopy height variables such as maximum height, average height, and quantiles, as well as point clouds derived from airborne LiDAR point clouds such as canopy coverage and canopy undulation. Characteristic variables can quantitatively describe the canopy distribution of forest vegetation.

In this study, three types of LiDAR variables were extracted at the plot level in Table 2: (1) Canopy height variables, including height maximum (H_{max}), height average (H_{mean}), and height quantile (H_p: p_{20}, p_{50}, p_{70}, p_{90}), height standard deviation (H_{SD}), height variation coefficient (H_{cv}), variance (H_{var}), slope (H_{ske}), and peak value (H_{kur}); (2) Canopy coverage (COV); (3) A variable that measures the relative shape of the Canopy Relief Ratio (CRR), which is used to describe the percentage of all echoes larger than the average height.

2.2.3. Field data

In order to improve the accuracy of the model, it is usually necessary to conduct field surveys in the research area, and use the ground-based measured data obtained from the survey to verify the model and correction accuracy. Field surveys and experiments were

Table 2. Description of characteristic variable.

Type	Feature	Describe
Canopy height variables	H_{max}	Maximum point cloud height
	H_{mean}	Average height of the point cloud
	H_p	The percentile height of the point cloud
	H_{SD}	Point cloud height standard deviation
	H_{cv}	Change coefficient of point cloud height
	H_{var}	Point cloud height variance
	H_{ske}	Point cloud height gradient
	H_{kur}	Peak point cloud height
Canopy coverage	COV	The ratio of the canopy echo area to the total wave area
Shape of the canopy	CRR	Canopy Relief Ratio

conducted in the Hengqin New District to collect information about vegetation-related parameters required for vegetation biomass estimation. The specific process is to use subjective estimation to determine the location of sample cells within the scope of the study area, so that they are distributed throughout the study area. For each tree sample point such as the forest, measure the diameter at breast height (DBH), plant height and other structural parameters of the single tree. An allometric equation is a non-destructive method and will be used to calculate the vegetation AGB by using the forest stand parameters: DBH and Height (*H*) (Equation (1)). The allometric equation which will be used in this research was formulated by Chave et al. (2014). It was found to be the best fit pan-tropic model for biomass estimation.

$$AGB_{forest} = 0.0673 \times (\rho D^2 H) \times 0.976 \tag{1}$$

Among them, the value of ρ is 0.375, D represents the DBH, and H represents the tree height.

For grassland and low bush sample points, use the SUNSCAN canopy analysis to measure the LAI value of the sample points (Equation (2)). At the same time, basic information including vegetation types, land cover types, and sample point locations was also recorded. Samples were collected from the study area from 27 July to 7 August 2018.

$$AGB_{grass} = 44.396 \times (LAI) - 25.946 \tag{2}$$

During the on-site sampling process, a total of 200 sample points were collected. Because the accuracy of the model estimation depends on the quality of ground sampling data (Powell et al. 2010), and during the sampling process, there are problems such as human error, insufficient Global Positioning System (GPS) point accuracy, position offset, and position deviation when point data overlaps with area data. Before modelling, the collected data should be checked and standardized according to the actual characteristics, and abnormal data in orthogonal data should be eliminated (B. Xu et al. 2008) to ensure the reliability and accuracy of data. Finally, 164 sample data were obtained.

As mentioned before, we use the pre-processed image and sampling points for vegetation analysis to obtain the spectral characteristics of vegetation growth under different grassland management treatments, combined with the biomass parameters such as plant height and DBH collected on the field and the use of the parameters extracted from LiDAR are used for subsequent estimation and inversion.

2.3. Urban vegetation extraction

The accuracy of the interpretation is related to the uniformity of the vegetation surface under investigation (Szantoi et al. 2017). According to the high-resolution remote-sensing images of the study area and the field land cover, the location information of the GPS measurement points is used to mark the geographic location of the uncertain category. The land cover types of Hengqin are classified, and their potential surface features are constructed according to the types. Combined with the ground verification and manual correction of the landform feature distribution of the whole island, the 10 years land cover classification results of the study area were extracted through automatic processing. The

vegetation area in the study area was extracted, and the vegetation area was obtained for biomass estimation based on the pixel size.

In this paper, based on the object-oriented classification method, the multi-scale segmentation algorithm in Ecognition 9.0 is used for object-level segmentation of ground objects in the study area. The multi-scale segmentation algorithm is a bottom-up segmentation algorithm based on pair region fusion technology, which is mainly used to minimize the average difference and maximize the uniformity represented by the image object with a given resolution (Schneider 2012). The main thing is to determine the size of the appropriate segmentation scale to make the segmentation accuracy as high as possible. In the process of object-oriented segmentation, different segmentation scales should be used for different features, so that the extracted features are more complete. Use Worldview series data to divide the entire urban landscape into land cover types, including water, vegetation (forest and grass), bare land, road, building, and hard paving. The details are shown in Figure 2.

There are many kinds of vegetation in Hengqin. Vegetation classification is an important part of vegetation research and one of the most complicated problems. The classification of traditional vegetation is usually based on the appearance and structure characteristics, vegetation dynamic characteristics and habitat characteristics (Wan et al. 2019). High-resolution data from 2009 to 2018 were used to extract the vegetation areas within the study area, and the vegetation areas were divided into grassland and forest as two different vegetation areas for subsequent inversion. Combined with pixel size, the vegetation area in the study area was obtained for the inversion of urban vegetation biomass.

2.4. AGB *model*

2.4.1. *Calculation of biomass relevant characteristic*

Extracting geological factors related to biomass to participate in biomass estimation is an effective method to improve the accuracy of estimation (Corona et al. 2014). The model variables selected in the study mainly include wave band, vegetation index, and texture feature. The remote-sensing related factors mainly select the original bands that have a high correlation with the feature of the ground features. Through image pre-processing and reference to existing vegetation index studies, 10 vegetation indices were selected,
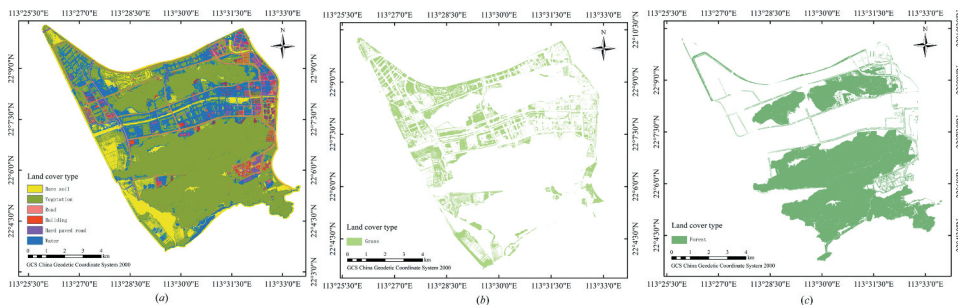

Figure 2. (*a*) Map for land cover derived from the worldview-3 image. (*b*) Map of the grass district. (*c*) Map of the forest district.

Table 3. Description of characteristic variable.

Feature	Describe	Feature	Describe
B_2	Blue band	MSAVI	$\dfrac{(2B_5+1-\sqrt{(2B_5+1)^2-8(B_5-B_4)})}{2}$
B_3	Green band	ARVI	$(B_5-B_4)/(B_5+B_4+0.5\times(B_2-B_4))/(B_5+B_4-0.5\times(B_2-B_4))$
B_4	Red band	OSAVI	$(B_5-B_4)/(B_5+B_4-0.16)$
B_5	NIR band	ME	$\sum_{i,j=0}^{N-1} i\times p_{i,j}$
NDVI	$(B_5-B_4)/(B_5+B_4)$	VAR	$\sum_{i,j=0}^{N-1} i\times p_{i,j}\times(i-ME)^2$
RVI	B_5/B_4	HO	$\sum_{i,j=0}^{N-1}\dfrac{p_{i,j}}{1+(i-j)^2}$
GNDVI	$(B_5-B_3)/(B_5+B_3)$	CO	$\sum_{i,j=0}^{N-1} i\times p_{i,j}\times(i-j)^2$
EVI	$(2.5\times(B_5-B_4))/(B_5+(6\times B_4-7.5\times B_2)+1)$	DI	$\sum_{i,j=0}^{N-1} i\times p_{i,j}\times|i-j|$
VI_{green}	$(B_3-B_4)/(B_3+B_4)$	EN	$\sum_{i,j=0}^{N-1} i\times p_{i,j}\times(-\ln p_{i,j})$
TVI	$\sqrt{NDVI+0.5}$	SM	$\sum_{i,j=0}^{N-1} i\times p_{i,j}^2$
SAVI	$1.5\times(B_5-B_4)/(B_5+B_4+0.5)$	COR	$\sum_{i,j=0}^{N-1} i\times p_{i,j}\times\left[\dfrac{(i-ME)(j-ME)}{\sqrt{VA_i}\times\sqrt{VA_j}}\right]$

[a]V_{ij} represents the pixel brightness value at the i row and j column, and N represents the size or size of the moving window when calculating the texture measure.

including Normalized Difference Vegetation Index (NDVI), Ratio Vegetation Index (RVI), Enhanced Vegetation Index (EVI), the variant of the NDVI that uses the green band (GNDVI), Soil-Adjusted Vegetation Index (SAVI), Modified Soil-Adjusted Vegetation Index (MSAVI), Optimized Soil-Adjusted Vegetation Index (OSAVI), Atmospherically Resistant Vegetation Index (ARVI), Temperature Vegetation Index (TVI), and Green Vegetation Index (VI$_{green}$), and select the corresponding Blue band (B_2), the Green band (B_3), the Red band (B_4) and the Near-infrared band (B_5). Texture feature variables include eight textures including ME (Mean), VAR (Variance), HO (Homogeneity), CO (Contrast), DI (Dissimilarity), EN (Entropy), SM (Second Moment) and COR (Correlation) (Table 3). Among them, the grey level co-occurrence matrix parameter is set to 3×3 and the grey level quantization level is 64.

Based on the location information of the sampling points, the band values, various vegetation index values and texture feature values of each sampling point are extracted from the selected feature layer, and the extracted variable values are normalized to improve the estimation accuracy (Zhang et al. 2019). In these analyses, the metrics were used as an independent variable while urban vegetation biomass was used as dependent variables. In this study, the Pearson correlation coefficient (r) for regression analyses between the metrics and urban vegetation biomass was calculated to assess the relationships. All statistical analyses were carried out with the standard statistical software SPSS19.0.

2.4.2. Estimation method

In order to explore relationship between the metrics and urban vegetation biomass for estimating urban vegetation, correlation analyses between the measurements of the set of urban vegetation biomass and corresponding. Then, the corresponding regression models between the metrics and urban vegetation were also established to uncover quantitative relationships between them. In the experiment, five types of prediction models were selected for inversion: stepwise linear regression (SLR), K-nearest neighbor (KNN), backpropagation neural network (BPNN), support vector regression (SVR), and random forest (RF) (Belgiu and Drăguţ 2016). The verification accuracy of each model determined the best biomass inversion model. In actual treatment, we divided the vegetation part of the study area into forest area and grassland area. At the same time, the two different vegetation geomorphologies were analysed and sampled. Established their own biomass inversion models, and obtained the final biomass. The specific process is shown in Figure 3.

Simple linear regression is a linear regression model with a single explanatory variable. That is, it concerns two-dimensional sample points with one independent variable and one dependent variable and finds a linear function that, as accurately as possible, predicts the dependent variable values as a function of the independent variables. Ullah et al. (2012) used this method to estimate grassland biomass and proved the linear relationship between various related factors and grassland biomass. KNN is the estimated value of the pixel to be measured is obtained by the weighted average of the corresponding attribute values of K reference points. Many experiments have proved that KNN can be well applied to an inversion of vegetation conditions.

BPNN is a feedforward neural computing model trained based on the error forward propagation algorithm. The backpropagation of the error signal is used to adjust the
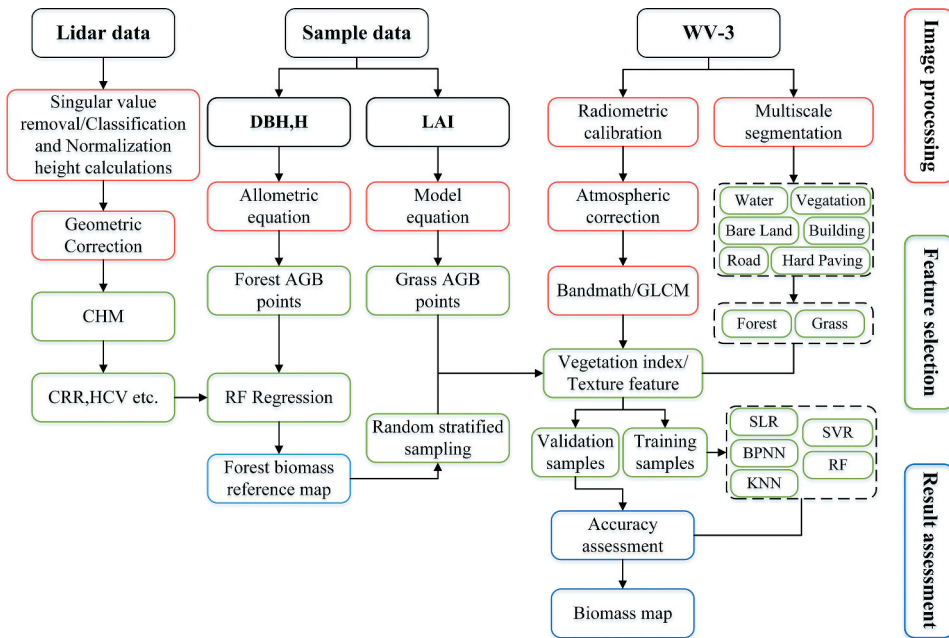
Figure 3. Two-stage inversion method for estimation of urban aboveground biomass.

weights and offsets of the network structure so that the output value of the network approaches the expected value. It has excellent non-linear mapping ability, generalization ability, and fault tolerance ability, showing superiority in terms of classification and prediction, and has become the most widely used artificial neural network. In recent years, BPNN model has made preliminary research advances in the application of chlorophyll content estimation models. This method can perform a non-linear mapping between any three-dimensional data input and output vectors, which is similar to any non-linear continuous system. At the same time, it also provides technical means for forest tree species classification research.

SVR works similarly to the support vector machine (SVM) classification. It can be said that SVR is an adaptive form of SVM when the dependent variable is not a classification but a number (Mountrakis, Im, and Ogole 2011). The main benefit of using SVR is that it is non-parametric. The nonlinear kernel function is used to transform the input sample data into another high-dimensional feature space, and the regression function is constructed in that high-dimensional feature space. Compared with Artificial Neural Network (ANN) and KNN algorithms, SVR is good at solving small sample, nonlinear and high-dimensional problems, which can overcome the problem of excessive learning and insufficient data in traditional estimation algorithms.

RF is based on self-service resampling technology (TTemesgen and Ver Hoef 2015). For the regression problem, average the estimated value of each tree to get the final estimated value. As a kind of nonparametric model, a random forest can effectively avoid the complex relationship between dependent variables and many independent variables. The classification and prediction speed of the model is fast, without adjusting most parameters, it can effectively process a large number of sample data, without

overfitting phenomenon, strong anti-noise ability and the importance of classification or prediction variables. It is very suitable for processing table data with fewer than hundreds of categories of digital features or classification features. It has been widely used in the fields of ecology and biology.

2.4.3. Training and validation data

The collection of ground data is often difficult, and the sample size of general measured data is very small. Before inverting the vegetation biomass in the entire study area, we first used the measured sample data and the extracted LiDAR variables to perform the first biomass inversion in the aerial image area. Later, a stratified random sampling method was used to expand the true value of the biomass, and then the optical data variables were used to estimate and invert the biomass in the study area.

The hierarchical random sampling method is used to select the training and verification sample set required for biomass estimation in the simulated LiDAR coverage area. The sample selection does not take into account the research area outside the simulated data. Because the tree height can directly characterize the forest structure and growth status, the LiDAR height variables H_{mean} and H_{SD} are selected as prior knowledge to implement layering on all candidate sample data (that is, all simulated coverage area data). First, prepare the data of the simulated band coverage area, including the AGB value in the biomass baseline map and its corresponding predictor value (including all optical variables, H_{mean} and H_{SD}). Secondly, the above data set is arranged in ascending order according to H_{mean}, and then equally divided into 10 data layers of the same size; then, each data layer is arranged in ascending order according to H_{SD}, and then equally divided into 4 equal parts, thereby generating 40 in total data layers of the same size. Finally, 20 samples are randomly selected from each data layer, and a total of 800 sample data can be obtained, which are randomly divided into training and verification sample sets according to a 3:1 ratio.

Based on the RF algorithm, the biomass estimation model was constructed by using AGB training sample data and LiDAR variables to obtain the biomass distribution result map of the study area. The finally selected LiDAR variables were used to construct the biomass estimation model and a biomass distribution result map that obtained as a reference map for subsequent inversion models.

2.4.4. Accuracy assessment

Biomass inversion model accuracy evaluation, that is, the accuracy of the inversion results requires the use of relevant verification indicators. Three verification indicators are used, namely the coefficient of determination (R^2), root-mean-square error (RMSE) (Equation (3)), and relative root mean square error (RMSEr) (Equation (4)). The most accurate prediction model is used as the final selected inversion model. Calculated as follows:

$$RMSE = \sqrt{\frac{\sum_{i=1}^{n} (y_{i,meas} - y_{i,est})^2}{N}} \tag{3}$$

$$RMSEr = \frac{\sum_{i=1}^{n} \frac{|y_{i,meas} - y_{i,est}|}{y_{i,meas}}}{N} \tag{4}$$

In the formula, $y_{i,meas}$ and $y_{i,est}$ respectively represent the measured and estimated values of the samples, n is the number of samples, and N is the number of reserved samples. The smaller the RMSE, the better the fit R^2 represents the degree of fit between the predicted value of the regression analysis trend line and the corresponding measured data. When the R^2 of the trend line approaches 1, the credibility is the highest.

3. Results

3.1. AGB *statistics analysis in major vegetation type*

In order to evaluate the closeness between vegetation biomass and characteristic variables that can be used to construct a remote-sensing estimation model are selected, and correlation analysis is performed between characteristic factors and biomass. Correlation analysis is a process of determining the closeness of the dependency relationship between variables by means of several analysis indicators such as correlation coefficients and correlation indexes. In this study, R^2 for regression analyses between factors and urban vegetation biomass was calculated to assess the relationships. All statistical analyses were carried out with the standard statistical software, SPSS.

The correlation between biomass and characteristic factors is shown in Table 4 and Table 5. There is a positive correlation between biomass and multiple vegetation indices, and there is a negative correlation with the band factor part, and some factors are not significant. According to the correlation analysis between biomass and each characteristic factor, it can be seen that the correlation between vegetation index and biomass is significant.

3.2. *Comparative analysis of urban vegetation estimation model*

A total of 164 sample data were obtained and randomly divided into test samples ($T = 124$) and verification samples ($V = 40$) in a ratio of 3:1. Table 6 summarizes the model accuracy results obtained using different regression methods. In all models, RF is superior to other methods. In terms of cross-validation, the RF-AGB model usually results

Table 4. The relationship between independent variable and grass biomass.

Feature	r	Feature	r
B_2	−0.533**	EVI	0.489**
B_3	−0.525**	VIgreen	0.340**
B_4	−0.553**	SAVI	0.649**
B_5	−0.600**	MSAVI	0.637**
NDVI	0.649**	ARVI	0.651**
RVI	0.579**	OSAVI	0.649**
TVI	0.388**	GNDVI	0.550**
ME	−0.113*	DI	0.294**
VAR	0.310	EN	0.041
HO	−0.198*	SM	−0.031
CO	0.295**	COR	−0.265**

[a]**: Significantly correlated at the 0.01 level.
[b]*: Significantly correlated at the 0.05 level.

Table 5. The relationship between independent variable and forest biomass.

Feature	r	Feature	r
B_2	−0.434**	EVI	0.655**
B_3	−0.453**	VIgreen	0.598**
B_4	−0.540**	SAVI	0.751**
B_5	0.167**	MSAVI	0.713**
NDVI	0.751**	ARVI	0.746**
RVI	0.717**	OSAVI	0.751**
TVI	0.572**	GNDVI	0.639**
ME	0.070	DI	0.373**
VAR	0.203**	EN	0.264**
HO	−0.404**	SM	−0.240**
CO	0.250**	COR	−0.102*

a**: Significantly correlated at the 0.01 level.
b*: Significantly correlated at the 0.05 level.

in higher R^2 and smaller RMSE (R^2 = 0.6913, RMSE = 26.98 Mg ha^{-1}, RMSEr = 0.4418). In terms of model accuracy and cross-validation, the SLR-AGB model has the worst performance in terms of R^2 and RMSE. Therefore, in the experiment, WV-2 image data are used as the input data, and RF is the prediction method to estimate the vegetation AGB on the regional scale.

To further validate the selected model, the remaining 40 plots were used for independent validation (Table 6). The predicted forest AGB value is the median of 124 bootstrap estimates. The results showed that R^2 was 0.5489 and RMSE was 32.61 Mg ha^{-1}, which was within the acceptable range. To further validate the selected model, the remaining 40 plots were used for independent validation (Figure 4). The predicted forest AGB value is the median of 124 bootstrap estimates. The results showed that R^2 was 0.5252 and RMSE was 38.58 Mg ha^{-1}, which was within the acceptable range.

The relationship between AGB and the predicted biomass in an RF model shown in Figure 4. The distribution of the scattered points is concentrated near the 1: 1 line, but this model underestimates the forest AGB with a higher AGB (0 to 180 Mg ha^{-1}) and the grass AGB with a higher AGB (0 to 140 Mg ha^{-1}). The model accuracy results of RF AGB models created with different sample sizes (Figure 4(a) and (b)) show that increasing the sample size results in an increase in R^2, a decrease in RMSE, and a decrease in the range of variation, which means that the established model is more stable.

Experimental results show that the RF model performs optimally in all scenarios, which has the same conclusion as the previous studies. Maack et al. (2015) used the spectrum, texture and photogrammetric information of Pleiades and WV-2, combined with four non-

Table 6. Comparison of precision result of five model.

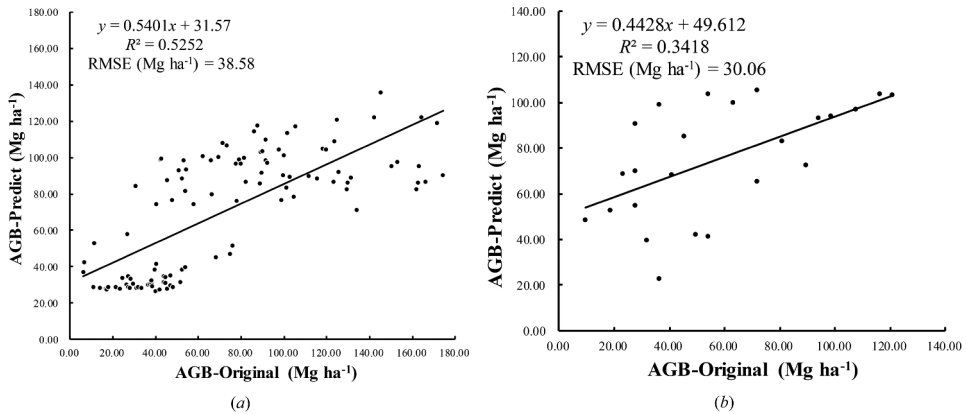| Model	R^2	RMSE (Mg ha^{-1})	RMSEr
SLR	0.5489	32.61	0.5341
KNN	0.6802	27.46	0.4497
BPNN	0.6077	30.41	0.4981
SVR	0.5788	31.52	0.5161
RF	0.6913	26.98	0.4418

Figure 4. (*a*) Forest and (*b*) Grass AGB verification result.

parametric models such as RF to estimate forest AGB, and found that RF algorithm achieved the highest estimation accuracy.

3.3. *Spatial and temporal distribution of* AGB

The advantage of remote-sensing data is that it can provide ground spectral characteristics and image information for a long time, and realize dynamic change monitoring (Powell et al. 2010). Due to the periodicity and continuity of remote-sensing data, dynamic monitoring is one of the most important application of satellite remote sensing. The study of interannual change can reflect the growth of vegetation over a period of time, and use the obtained remote-sensing image data to estimate the biomass of the study area on the spatial and temporal scales. The use of multi-temporal high-resolution remote-sensing images can perform change analysis, thereby reflecting the development of regional urban construction and the simultaneous and coordinated development of green space. According to the map of all vegetation inversion results of the study area from 2009 to 2018 (Figure 5), the total annual biomass of the study area can be calculated.

4. Discussion

4.1. AGB *in different area*

The relevant index factors are extracted from the image data and modelled with the biomass to obtain the vegetation biomass distribution map of the study area. Secondly, the relationship between the index and AGB in the entire study area and different vegetation classifications is analysed. Finally, it is shown that results in a range of environmental influences on urban vegetation. The range of ground data sampling has a great influence on the inversion of the following models. For example, if the sampled data are generally small, the final result may be an underestimate. On the other hand, if the sampled data are generally large, the final estimation results may be based on overestimation. When the model is retrieved in a large area, the variation range of AGB is large due to the different coverage of vegetation, which will lead to the
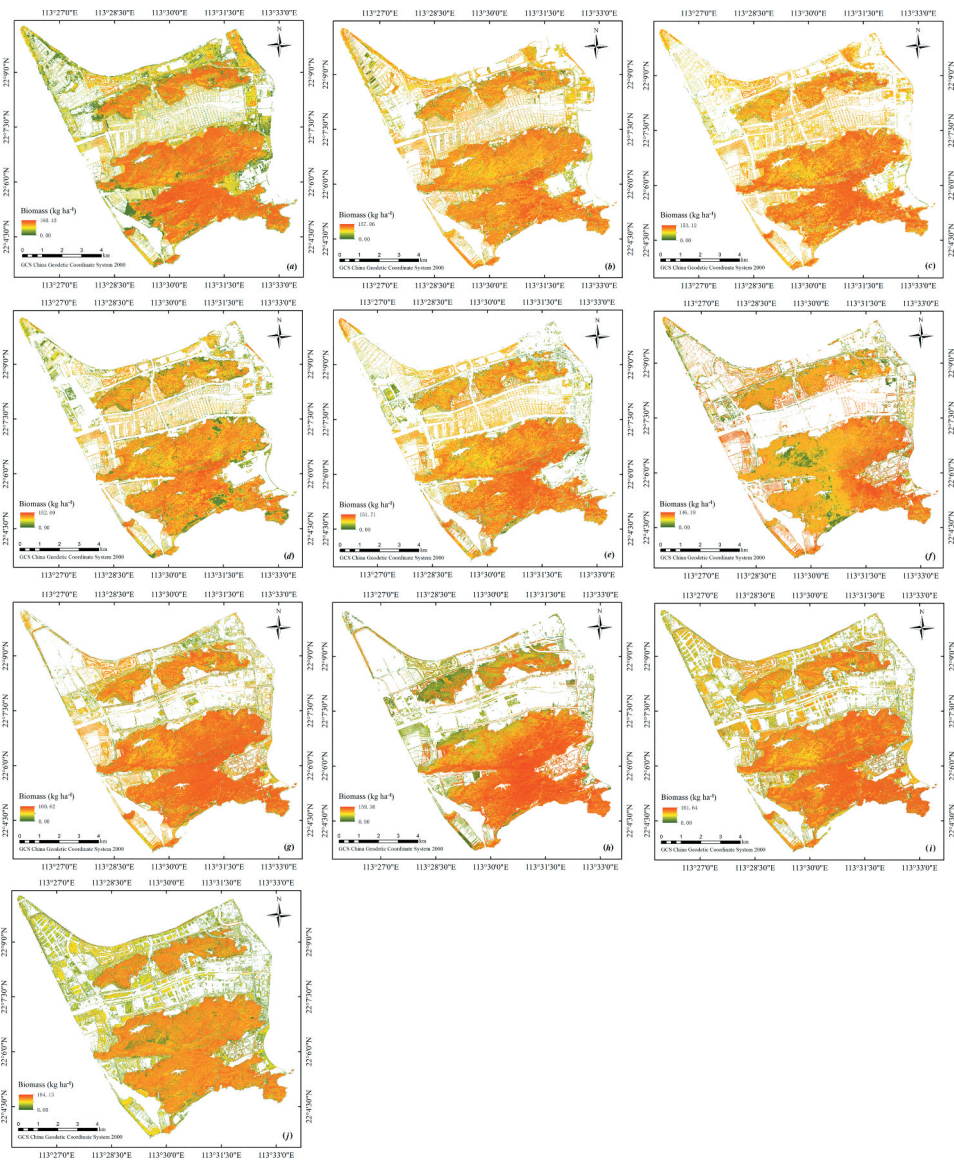
Figure 5. (*a*) 2009 (*b*) 2010 (*c*) 2011 (*d*) 2012 (*e*) 2013 (*f*) 2014 (*g*) 2015 (*h*) 2016 (*i*) 2017 (*j*) 2018. Biomass distribution map of urban vegetation in the study area from 2009 to 2018.

underestimation or overestimation at a later stage due to the uneven sampling. Both the underestimation of pixel-level AGB and forest cover area caused the underestimation of total AGB estimates.

As far as natural conditions are concerned, mountain forests have more tree species with a long age and high density. The trees have long planting time, large growth space, and good development status, and the proportion of large-diameter trees is high. In the central city area, although the forest is planted for a long time, the growth rate is fast, and the leaf biomass density is high, with the comprehensive and rapid development of the

city, the development and use of land, the building land takes up a large area of land and the limited area of the central city area (Shao et al. 2020c). The forest area in the area is significantly smaller than the forest area in mountainous areas. With the development and construction of cities, urban vegetation biomass has experienced a process of the first reduction and then increase. Due to the popularity and scale of the eco-city concept, the area of urban green space has also increased year after year.

4.2. Analysis of difference of feature types

It can be seen from the statistical results that from 2009 to 2014 (Figure 6), the total vegetation biomass in the study area decreased year by year. Because urban construction and urban expansion are carried out by policy implementation (Shao Z et al. 2020a). The expansion of building area has led to the destruction of some vegetation areas, the area of grassland in the urban area has been greatly reduced, and the storage of grassland has been greatly reduced. This is also the destruction of the natural ecology in the early stage of urban construction. In 2014 to 2018, the vegetation showed an overall growth trend, which is also closely related to the development of ecological island construction.

Compared with grass ecosystem, forests have a long life cycle, a fairly complex hierarchy, the highest biomass, and growth, etc., because of human deforestation, the forest area is getting smaller and smaller, and the size of forest biomass affected by various factors such as photosynthesis, respiration, and human activities. Therefore, changes in forest biomass indirectly reflect the impacts of forest community succession and natural disturbances, human activities, climate change, and air pollution. Analysis of forest biomass can reflect the quantitative relationship between matter and energy in forest ecosystems, and the relationship
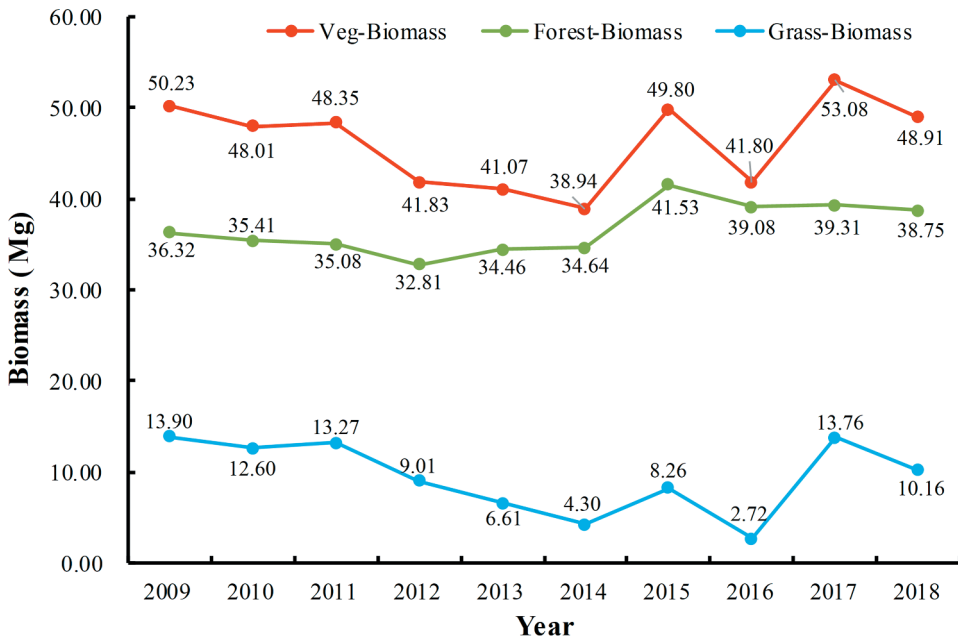

Figure 6. Biomass statistical map of vegetation area in 10 years.

between biomass and ecological elements. It is an important indicator for evaluating the function and structure of forest ecosystems. Forest biomass and carbon storage can not only indicate the forest's own use-value and management level but also explain the relationship between forest and its environment in terms of the material cycle and energy flow, which can provide a theoretical basis for sustainable use of forest resources.

By analysing the distribution of vegetation biomass in the study area, it can be found that the vegetation changes with environmental conditions. For example, the biomass and density of urban forest areas will be significantly higher than the surrounding areas such as sidewalks and park areas. The spatial distribution of the average biomass density of vegetation throughout the study area is high in mountains such as forests and low in central urban areas. Because urban areas are mostly covered by impervious surfaces (such as roads, buildings, etc.), and urban green space patches are mostly broken, the landscape heterogeneity is high, which makes the carbon absorption function not only inferior to that of dense alpine forests. At the same time, forest biomass is closely related to many biological and non-biological factors, such as regional hydrothermal conditions, soil conditions, forest types, ages, dominant species composition, living tree density, etc. These factors will affect biomass change and distribution.

4.3. Existing problems and prospective

Urban forest biomass and its spatial distribution pattern of accurate, rapid, efficient monitoring and estimation, not only is the basis of the understanding of forest carbon cycle and energy flow, or to measure urban forest play a role of ecological regulation, environmental protection, and resources to repair, forest cover is also the research status and the basis of urban ecological construction.

Optics, radar, and LiDAR data have their own advantages and disadvantages. It is important to combine appropriate methods to improve the accuracy of biomass estimation. LiDAR data can effectively estimate forest structure parameters, but because most LiDAR systems have only a single band three-dimensional (3D) structure Information (He et al. 2013), they do not provide sufficient vegetation spectral information. Optical data can provide rich spectral information, but the relationship between optical reflectance and canopy structure characteristics is prone to saturation problems. Therefore, LiDAR and optical data are highly complementary. The next step is how to integrate LiDAR and multispectral data to estimate urban vegetation.

We developed, evaluated, and compared the accuracy and performance of five different models in this study on forest AGB estimates. Machine learning also has its advantages and disadvantages. Machine learning has the advantage of being able to handle complex, potentially nonlinear relationships between AGB and other variables. However, the initial samples of machine learning are randomly selected, which may lead to differences in the results of each operation of the model. In addition, machine learning uses the average value of all regression trees in the calculation, which may result in overestimating the lower value and underestimating the higher value.

There are many kinds of urban vegetation. It is one of the most complicated problems to classify and classify vegetation from the perspective of traditional optical images. Through the combination of spectral characteristics of different vegetation and hyperspectral remote-sensing images, the rapid classification of urban vegetation types and the monitoring of vegetation type changes are also one of the main directions of future work.

5. Conclusions

The major contribution of this study is the assessment of urban vegetative above biomass by integrating terrestrial AGB observations and integrating multi-source remote-sensing data. Urban vegetation is divided into grassland and forestland, and the range of this type of vegetation is precisely extracted by the classification method. The parameter estimation based on LiDAR data is used as the alternative data of traditional forest inventory data. In the experiment, the biomass extracted from LiDAR was sampled randomly in layers, and when combined with optical data to obtain the best RF-based vegetation inversion model through the inversion of five models. The results show that our prediction graph not only captures the quantity and spatial distribution of urban vegetation AGB but also shows lower RMSE and deviation.

Acknowledgements

Disclosure statement

No potential conflict of interest was reported by the authors.

Funding

References

Ali, I., F. Greifeneder, J. Stamenkovic, M. Neumann, and C. Notarnicola. 2015. "Review of Machine Learning Approaches for Biomass and Soil Moisture Retrievals from Remote Sensing Data." *Remote Sensing* 7 (12): 16398–16421. doi:10.3390/rs71215841.

Belgiu, M., and L. Drăguţ. 2016. "Random Forest in Remote Sensing: A Review of Applications and Future Directions." *ISPRS Journal of Photogrammetry and Remote Sensing* 114: 24–31. doi:10.1016/j.isprsjprs.2016.01.011.

Chave, J., M. Réjou-Méchain, A. Búrquez, E. Chidumayo, M. S. Colgan, W. B. Delitti, … M. Henry. 2014. "Improved Allometric Models to Estimate the Aboveground Biomass of Tropical Trees." *Global Change Biology* 20 (10): 3177–3190. doi:10.1111/gcb.12629.

Clark, M. L. 2020. "Comparison of Multi-seasonal Landsat 8, Sentinel-2 and Hyperspectral Images for Mapping Forest Alliances in Northern California." *ISPRS Journal of Photogrammetry and Remote Sensing* 159: 26–40. doi:10.1016/j.isprsjprs.2019.11.007.

Corona, P., L. Fattorini, S. Franceschi, G. Chirici, F. Maselli, and L. Secondi. 2014. "Mapping by Spatial Predictors Exploiting Remotely Sensed and Ground Data: A Comparative Design-based Perspective." *Remote Sensing of Environment* 152: 29–37. doi:10.1016/j.rse.2014.05.011.

Fung, T., and W. Siu. 2000. "Environmental Quality and Its Changes, an Analysis Using NDVI." *International Journal of Remote Sensing* 21 (5): 1011–1024. doi:10.1080/014311600210407.

Gao, T., B. Xu, X. Yang, Y. Jin, H. Ma, J. Li, and H. Yu. 2013. "Using MODIS Time Series Data to Estimate Aboveground Biomass and Its Spatio-temporal Variation in Inner Mongolia's Grassland between 2001 and 2011." *International Journal of Remote Sensing* 34 (21): 7796–7810. doi:10.1080/01431161.2013.823000.

Guo, Y., Z. Li, X. Zhang, E. X. Chen, L. Bai, X. Tian, . . . W. Li. 2012. "Optimal Support Vector Machines for Forest Above-ground Biomass Estimation from Multisource Remote Sensing Data". In *2012 IEEE International Geoscience and Remote Sensing Symposium* (pp. 6388–6391). IEEE. doi: 10.1109/IGARSS.2012.6352721.

He, Q., E. Chen, R. An, and Y. Li. 2013. "Above-ground Biomass and Biomass Components Estimation Using LiDAR Data in a Coniferous Forest." *Forests* 4 (4): 984–1002. doi:10.3390/f4040984.

Jin, Y., X. Yang, J. Qiu, J. Li, T. Gao, Q. Wu, . . . B. Xu. 2014. "Remote Sensing-based Biomass Estimation and Its Spatio-temporal Variations in Temperate Grassland, Northern China." *Remote Sensing* 6 (2): 1496–1513. doi:10.3390/rs6021496.

Johnson, B. A. 2013. "High-resolution Urban Land-cover Classification Using a Competitive Multi-scale Object-based Approach." *Remote Sensing Letters* 4 (2): 131–140. doi:10.1080/2150704X.2012.705440.

Kumar, L., and O. Mutanga 2017. "Remote Sensing of Above-ground Biomass". doi:10.3390/rs9090935.

Li, F., L. Jiang, X. Wang, X. Zhang, J. Zheng, and Q. Zhao. 2013. "Estimating Grassland Aboveground Biomass Using Multitemporal MODIS Data in the West Songnen Plain, China." *Journal of Applied Remote Sensing* 7 (1): 073546. doi:10.1117/1.JRS.7.073546.

Li, X., W. Y. Chen, G. Sanesi, and R. Lafortezza. 2019. "Remote Sensing in Urban Forestry: Recent Applications and Future Directions." *Remote Sensing* 11 (10): 1144. doi:10.3390/rs11101144.

Liu, X., F. Pei, Y. Wen, X. Li, S. Wang, C. Wu, . . . J. Liu. 2019. "Global Urban Expansion Offsets Climate-driven Increases in Terrestrial Net Primary Productivity." *Nature Communications* 10 (1): 1–8. doi:10.1038/s41467-019-13462-1.

Lucas, R. M., A. C. Lee, and P. J. Bunting. 2008. "Retrieving Forest Biomass through Integration of CASI and LiDAR Data." *International Journal of Remote Sensing* 29 (5): 1553–1577. doi:10.1080/01431160701736497.

Maack, J., T. Kattenborn, F. E. Fassnacht, F. Enßle, J. Hernández, P. Corvalán, and B. Koch. 2015. "Modeling Forest Biomass Using Very-High-Resolution data-Combining Textural, Spectral and Photogrammetric Predictors Derived from Spaceborne Stereo Images." *European Journal of Remote Sensing* 48 (1): 245–261. doi:10.5721/EuJRS20154814.

Mincey, S. K., M. Schmitt-Harsh, and R. Thurau. 2013. "Zoning, Land Use, and Urban Tree Canopy Cover: The Importance of Scale." *Urban Forestry & Urban Greening* 12 (2): 191–199. doi:10.1016/j.ufug.2012.12.005.

Mountrakis, G., J. Im, and C. Ogole. 2011. "Support Vector Machines in Remote Sensing: A Review." *ISPRS Journal of Photogrammetry and Remote Sensing* 66 (3): 247–259. doi:10.1016/j.isprsjprs.2010.11.001.

Mutanga, O., E. Adam, and M. A. Cho. 2012. "High Density Biomass Estimation for Wetland Vegetation Using WorldView-2 Imagery and Random Forest Regression Algorithm." *International Journal of Applied Earth Observation and Geoinformation* 18: 399–406. doi:10.1016/j.jag.2012.03.012.

Muukkonen, P., and J. Heiskanen. 2005. "Estimating Biomass for Boreal Forests Using ASTER Satellite Data Combined with Standwise Forest Inventory Data." *Remote Sensing of Environment* 99 (4): 434–447. doi:10.1016/j.rse.2005.09.

Powell, S. L., W. B. Cohen, S. P. Healey, R. E. Kennedy, G. G. Moisen, K. B. Pierce, and J. L. Ohmann. 2010. "Quantification of Live Aboveground Forest Biomass Dynamics with Landsat Time-series and Field Inventory Data: A Comparison of Empirical Modeling Approaches." *Remote Sensing of Environment* 114 (5): 1053–1068. doi:10.1016/j.rse.2009.12.018.

Rafiee, R., A. S. Mahiny, and N. Khorasani. 2009. "Assessment of Changes in Urban Green Spaces of Mashad City Using Satellite Data." *International Journal of Applied Earth Observation and Geoinformation* 11 (6): 431–438. doi:10.1016/j.jag.2009.08.005.

Ren, Z., R. Pu, H. Zheng, D. Zhang, and X. He. 2017. "Spatiotemporal Analyses of Urban Vegetation Structural Attributes Using Multitemporal Landsat TM Data and Field Measurements." *Annals of Forest Science* 74 (3): 54. doi:10.1007/s13595-017-0654-x.

Schneider, A. 2012. "Monitoring Land Cover Change in Urban and Peri-urban Areas Using Dense Time Stacks of Landsat Satellite Data and a Data Mining Approach." *Remote Sensing of Environment* 124: 689–704. doi:10.1016/j.rse.2012.06.006.

Shao, Z., C. Li, D. Li, O. Altan, L. Zhang, and L. Ding. 2020a. "An Accurate Matching Method for Projecting Vector Data into Surveillance Video to Monitor and Protect Cultivated Land." ISPRS International Journal of Geo-Information 9 (7): 448. doi:10.3390/ijgi9070448

Shao, Z., L. Ding, D. Li, O. Altan, M. Huq, and C. Li. 2020b. "Exploring the Relationship between Urbanization and Ecological Environment Using Remote Sensing Images and Statistical Data: A Case Study in the Yangtze River Delta, China." Sustainability 12 (14): 5620. doi:10.3390/su12145620

Shao, Z., L. Zhang, and L. Wang. 2017. "Stacked Sparse Autoencoder Modeling Using the Synergy of Airborne LiDAR and Satellite Optical and SAR Data to Map Forest Above-ground Biomass." *IEEE Journal of Selected Topics in Applied Earth Observations and Remote Sensing* 10 (12): 5569–5582. doi:10.1109/JSTARS.2017.2748341.

Shao, Z., P. Tang, Z. Wang, N. Saleem, S. Yam, and C. Sommai. 2020c. "BRRNet: A Fully Convolutional Neural Network for Automatic Building Extraction from High-Resolution Remote Sensing Images." *Remote Sensing* 12 (6): 1050. doi:10.3390/rs12061050.

Shao, Z., W. Zhou, X. Deng, M. Zhang, and Q. Cheng. 2020d. "Multilabel Remote Sensing Image Retrieval Based on Fully Convolutional Network." *IEEE Journal of Selected Topics in Applied Earth Observations and Remote Sensing* 13: 318–328. doi:10.1109/JSTARS.2019.2961634.

Szantoi, Z., S. E. Smith, G. Strona, L. P. Koh, and S. A. Wich. 2017. "Mapping Orangutan Habitat and Agricultural Areas Using Landsat OLI Imagery Augmented with Unmanned Aircraft System Aerial Photography." *International Journal of Remote Sensing* 38 (8–10): 2231–2245. doi:10.1080/01431161.2017.1280638.

Tao, Y., F. Li, R. Wang, and D. Zhao. 2013. "Research Progress in the Quantitative Methods of Urban Green Space Patterns." *Shengtai Xuebao/Acta Ecologica Sinica* 33 (8): 2330–2342.

Temesgen, H., and J. M. Ver Hoef. 2015. "Evaluation of the Spatial Linear Model, Random Forest and Gradient Nearest-neighbour Methods for Imputing Potential Productivity and Biomass of the Pacific Northwest Forests." *Forestry: An International Journal of Forest Research* 88 (1): 131–142. doi:10.1093/forestry/cpu036.

Ullah, S., Y. Si, M. Schlerf, A. K. Skidmore, M. Shafique, and I. A. Iqbal. 2012. "Estimation of Grassland Biomass and Nitrogen Using MERIS Data." *International Journal of Applied Earth Observation and Geoinformation* 19: 196–204. doi:10.1016/j.jag.2012.05.008.

Wallis, C. I., J. Homeier, J. Peña, R. Brandl, N. Farwig, and J. Bendix. 2019. "Modeling Tropical Montane Forest Biomass, Productivity and Canopy Traits with Multispectral Remote Sensing Data." *Remote Sensing of Environment* 225: 77–92. doi:10.1016/j.rse.2019.02.021.

Wan, R., P. Wang, X. Wang, X. Yao, and X. Dai. 2019. "Mapping Aboveground Biomass of Four Typical Vegetation Types in the Poyang Lake Wetlands Based on Random Forest Modelling and Landsat Images." *Frontiers in Plant Science* 10. doi:10.3389/fpls.2019.01281.

Wang, Z., G. Shen, Y. Zhu, C. Liu, Y. Han, and Y. Zhou 2015, July. "Spatiotemporal Dynamics of Urban Forest Biomass in Shanghai, China". In *2015 Fourth International Conference on Agro-Geoinformatics (Agro-geoinformatics)* (pp. 384–389). *IEEE*. doi: 10.1109/Agro-Geoinformatics.2015.7248154.

Willhauck, G., T. Schneider, R. De Kok, and U. Ammer 2000, July. "Comparison of Object Oriented Classification Techniques and Standard Image Analysis for the Use of Change Detection between SPOT Multispectral Satellite Images and Aerial Photos". *Proceedings of XIX ISPRS congress* (Vol.33, pp. 35–42). Amsterdam: IAPRS.

Wilson, J. S., M. Clay, E. Martin, D. Stuckey, and K. Vedder-Risch. 2003. "Evaluating Environmental Influences of Zoning in Urban Ecosystems with Remote Sensing." *Remote Sensing of Environment* 86 (3): 303–321. doi:10.1016/S0034-4257(03)00084-1.

Xu, B., X. C. Yang, W. G. Tao, Z. H. Qin, H. Q. Liu, J. M. Miao, and Y. Y. Bi. 2008. "MODIS-based Remote Sensing Monitoring of Grass Production in China." *International Journal of Remote Sensing* 29 (17–18): 5313–5327. doi:10.1080/01431160802036276.

Zhang, G., S. Ganguly, R. R. Nemani, M. A. White, C. Milesi, H. Hashimoto, … R. B. Myneni. 2014. "Estimation of Forest Aboveground Biomass in California Using Canopy Height and Leaf Area Index Estimated from Satellite Data." *Remote Sensing of Environment* 151: 44–56. doi:10.1016/j. rse.2014.01.025.

Zhang, L., Z. Shao, J. Liu, and Q. Cheng. 2019. "Deep Learning Based Retrieval of Forest Aboveground Biomass from Combined LiDAR and Landsat 8 Data." *Remote Sensing* 11 (12): 1459. doi:10.3390/ rs11121459

Zhang, R., X. Zhou, Z. Ouyang, V. Avitabile, J. Qi, J. Chen, and V. Giannico. 2019. "Estimating Aboveground Biomass in Subtropical Forests of China by Integrating Multisource Remote Sensing and Ground Data." *Remote Sensing of Environment* 232: 111341. doi:10.1016/j. rse.2019.111341

Zhou, J., B. Yu, and J. Qin. 2014. "Multi-level Spatial Analysis for Change Detection of Urban Vegetation at Individual Tree Scale." *Remote Sensing* 6 (9): 9086–9103. doi:10.3390/rs6099086.